Research Article

Mariano Febbo*, Sebastian P. Machado, Alejandro Oliva, Matias Ortiz and Nicolas Pereyra

Modelling of a piezoelectric beam with a full-bridge rectifier under arbitrary excitation: experimental validation

https://doi.org/10.1515/ehs-2022-0099
Received August 11, 2022; accepted November 26, 2022; published online January 4, 2023

Abstract: This paper presents a set of nonlinear differential equations to model a piezoelectric energy harvesting (PEH) system with a full-bridge waveform rectifier (FWR) under arbitrary base excitations. The PEH comprises a piezoelectric element modeled as a current source with a capacitor in parallel, which are connected with an inductor and a resistor. The inductor is proposed to smooth the current generated by the piezoelectric element under rapid mechanical variations and improve the convergence of the set of differential equations. The equations are obtained using piecewise linear modelling for the diodes. The main advantage of this piecewise linear modelling is considering different bias points to represent the nonlinear characteristics of real diodes. Numerical simulations are employed to obtain the optimum inductor value through a comparison with an analytical result, validated with experimental tests. A real case of random acceleration in a bike is applied to the PEH-FWR to evaluate the performance of the proposed equations. They are validated with experiments, a LTspice formulation and a numerical previous one. The proposed formulation can estimate the output DC voltage and energy for a large range of excitation frequencies, including resonant and nonresonant conditions and arbitrary or harmonically externally excited PEHs with FWR.

Keywords: full-bridge waveform rectifier; general differential equations; piecewise linear modelling; piezoelectric beam.

***Corresponding author: Mariano Febbo**, Departamento de Física, Instituto de Física del Sur (IFISUR), Consejo Nacional de Investigaciones Científicas y Técnicas (CONICET), Universidad Nacional del Sur (UNS), Av. Alem 1253, 8000 Bahía Blanca, Argentina, E-mail: mfebbo@uns.edu.ar
Sebastian P. Machado and Matias Ortiz, Grupo de Investigación en Multifísica Aplicada (GIMAP), Universidad Tecnológica Nacional FRBB (UTN), 11 de Abril 461, 8000 Bahía Blanca, and Consejo Nacional de Investigaciones Científicas y Técnicas (CONICET)
Alejandro Oliva, Departamento de Ingeniería Eléctrica y de Computadoras, Instituto de Investigaciones en Ingeniería Eléctrica (IIIE), Consejo Nacional de Investigaciones Científicas y Técnicas (CONICET), Universidad Nacional del Sur (UNS), San Andrés 800, 8000 Bahía Blanca, Argentina
Nicolas Pereyra, Departamento de Física, Universidad Nacional del Sur (UNS), Av. Alem 1253, 8000 Bahía Blanca, Argentina

Introduction

The necessity of new clean and environmentally friendly energy sources has been gaining increasing relevance in the last decades. In this sense, energy harvesting is one of the most promising alternatives to using fossil fuels for electric energy generation. Energy from ambient vibration can be harvested by mechanical-to-electrical transducers to supply low-power electronic devices. The power sources based on this type of energy are particularly attractive to energize real-time monitoring systems with a significant vibrational content (Anton and Sodano 2007; Beeby, Tudor, and White 2006; Erturk and Inman 2008, 2011; Fu et al. 2021; Harb 2011). Different mechanisms are available to perform the mechanical to electrical conversion: electrostatic (Peano and Tambosso 2005), electromagnetic (Saravia, Ramírez, and Gatti 2017), magnetostrictive (Mori et al. 2015), triboelectric (Fan, Tang, and Wang 2016), or piezoelectric (Gatti et al. 2018; Ramírez et al. 2019; Wang et al. 2020) transduction.

From all of the above, piezoelectric conversion has gained considerable interest by the ease of its implementation, high durability, and high power density. Several authors, which developed a theoretical framework using linear and nonlinear models, have carried out seminal contributions (Anton and Sodano 2007; Beeby, Tudor, and White 2006; Erturk and Inman 2008, 2011; Harb 2011; Machado et al. 2020) to study piezoelectric energy harvesters (PEH) that can be found in numerous applications since then (Chen, Wu, and Su 2020; Ramírez et al. 2017; Shahab, Zhao, and Erturk 2018; Upadrashta and Yang 2016).

The simplest PEH configuration consists of a cantilever beam with piezoceramic layers vibrating under base excitation. The structure is tuned to resonate with the external vibration (base input) to maximize the power generation. Theoretical and experimental works seeking to optimize the power generation of linear vibrating piezoelectric beams have received most of the attention in the literature (Erturk and Inman 2008, 2011). However, in the last decade, there has been an increasing interest in studying the nonlinear aspects of piezoelectric generators, such as their physical and material nonlinearities (Machado et al. 2020).

Physical (or mechanical) nonlinearities refer to a modification in the geometry or the addition of an external agent (e.g., a magnet, a sliding mass, stopper, etc.) to alter the characteristics of the frequency response. The main objective of their inclusion is to increase the frequency range where the harvester produces an appropriate amount of energy (relative to a resonant linear system). This is achieved via nonlinear effects including mono-, bi- or multi-stability (via Duffing nonlinearity and other higher order polynomial springs) (Mei et al. 2021; Stanton, McGehee, and Mann 2009; Wang et al. 2021), parametric oscillations (Daqaq et al. 2009; Jia and Seshia 2014; Kurmann et al. 2016), stochastic resonance (McInnes, Gorman, and Cartmell 2008; Moehils et al. 2009), mechanical stoppers (Kathpalia et al. 2018; Febbo and Machado 2022; Gu 2011), self-tuning mechanisms (Ayala-Garcia et al. 2010; Gu and Livermore 2011) and nonoscillatory mechanisms (Halim, Cho, and Park 2015; Roundy and Tola 2013).

Material nonlinearities refer to the intrinsic nonlinearity and dissipative behavior of piezoelectric materials (Machado et al. 2020). It is an experimental fact that when the amplitude of the base acceleration increases, linear models overestimate the electrical generation in a resonant condition; thus, they are inaccurate in modelling the response of piezoelectric systems that are excited with moderate to large excitations. For this reason, nonlinear constitutive equations were proposed instead of linear ones, such as in (Stanton et al. 2010). Other nonlinear topics that have been addressed by previous works are: the modelling of material nonlinearities such as the nonlinear elastic behavior (Joshi 1992), the nonlinear electromechanical coupling and ferroelectric hysteresis (Bertotti and Mayergoyz 2006; Goldschmidtboeing et al. 2011; Joshi 1992) and the nonlinear viscous dissipation (Stanton et al. 2010).

In order to convert the alternating current (AC) provided by a PEH to useful power, waveform rectifiers must be used to produce direct current (DC) to feed low-power electronic devices or charge electrical storage systems. The most common technique is connecting a full-bridge waveform rectifier between the PEH and the electric load (Roundy, Wright, and Rabaey 2003). Despite the fact that closed-formed analytical expressions have been developed for the DC voltage of a PEH under steady state base motion with ideal diodes (Shu and Lien 2006), few investigations have studied the transient response or the case of a general (random) excitation with nonideal circuit elements, so far.

Wu et al. (2009) presented analytical models for the transient behavior of several power harvesting circuit topologies during the charge of a large storage capacitor, assuming a sinusoidal motion of the piezoelectric beam. They presented time-dependent analytical expressions for the direct charging of a storage capacitor by a full waveform rectifier and compared them with measurements taken from an experimental circuit. They showed that the theoretical predictions are accurate when the losses in the circuit are considered in the model.

Clementino et al. (2014) introduced a comprehensive and simple model for both the electromechanical conversion of a clamped piezoelectric beam and a practical energy harvesting circuit composed by a full-bridge diode rectifier. Numerical simulations were performed using the commercial program Matlab/Simulink and compared with experimental tests using a sinusoidal waveform as the base excitation of the piezoelectric beam.

Wciślik and Strząbała (2016) described a nonlinear model of the full–bridge waveform rectifier with RC load under a sinusoidal input voltage. The model of the circuit was implemented and analyzed with MATLAB/Simulink. The system does not contain a piezoelectric transducer as the electrical power source, but it can be used to set the electromechanical differential equations needed for its study. Furthermore, the current–voltage characteristics for different values of capacitive load are presented, and the harmonic distortions of the currents and voltages in the considered circuit were also analyzed.

In 2019, Leadenham and Erturk (2020) presented a representation of the behavior of PEHs under material nonlinearities considering the nonlinear process of AC–DC conversion with nonideal circuit elements, such as real diodes. They studied a bimorph cantilever with piezoelectric laminates under sinusoidal base excitation. The solution, obtained in terms of a multiterm harmonic balance framework, can predict the ripple in the DC voltage as well as the amplitude-dependent dynamics of real diodes. The theoretical predictions were validated by comparing them with experimental data.

The present work addresses the problem of finding the differential equations that govern the behavior of a piezoelectric energy harvester undertaking the nonlinear

process of AC-DC conversion under an arbitrary excitation. The excitation amplitude is kept low enough in order to keep the system undergoing a linear behavior. This is carried out by selecting a very stiff system and providing a small acceleration excitation, so the geometric nonlinearities (stiffness hardening and inertial softening) and material nonlinearities can be neglected. Unlike other studies which treat the nonlinear process of AC-DC conversion together with other nonlinearities (material, for example, see Leadenham and Erturk (2020)), in this study, we concentrate on the former to isolate the problem with the aim of studying the effect of the nonlinear AC-DC process performed by an FWR comprising nonideal circuit elements, such as real diodes, in the voltage generation of a PEH.

The proposed model is validated by comparison with experimental data and computer simulation results, evidencing the importance of having a model that predicts the mechanical and electrical nonlinear and nonideal behavior of PEH-FWR for an arbitrary excitation and its output voltage and energy.

The article is organized as follows. After this introduction, a mathematical modelling of a PEH-FWR is presented in Mathematical modelling. Parameter estimation of L, diode model, experimental validations and comparisons introduces a numerical estimation for the inductance of the proposed model as a part of an identification and optimization process, using an experimental determination of the parameters of the piezoelectric beam. Real case acceleration excitation documents a real case of a random acceleration excitation applied to the PEH-FWR to test the theoretical predictions and to compare it to other numerical formulations of the same problem. Finally, Conclusions presents the conclusions.

Mathematical modelling

The selected physical system is a piezoelectric cantilever beam with interdigitated electrodes and piezofibers composite, manufactured by Advanced Cerametrics (PFCB-W24, see Figure 1). In order to model the selected PEH, a very stiff cantilever beam is considered in the experiments, neglecting the geometric nonlinearities (stiffness hardening and inertial softening). Also, the influence of material nonlinearity is not taken into account since small base excitation acceleration is applied to the system. Therefore, the modelling approach adopted in (Shu and Lien 2006) (linear model) is suitable under these circumstances.

Then, the system under study consists of a piezoelectric element modeled as a current source with a capacitor C_p in parallel, which is connected with an inductor L and resistor R_s (see Figure 2). When a current with fast di/dt passes through the nonlinear characteristic of the diodes it may increase the simulations time and even cause the simulation to stop. The inductor, L, is proposed to smooth the current generated by the piezoelectric element under rapid mechanical variations and improve the convergence of the set of differential equations; its value is determined for the best fit of the results. The harvesting circuit is completed with the full−bridge waveform rectifier loaded by the capacitor C and the resistor R, where the resistor R_d accounts for the internal resistance of the diode ($R_s = 2R_d$).

In order to model the system, the following equations are proposed:

$$\ddot{q}(t) + \mu\dot{q}(t) + \omega_0^2 q(t) - \vartheta v(t) = \Gamma a(t) \tag{1}$$

$$C_p \frac{dv(t)}{dt} + \vartheta\beta\,\dot{q}(t) = -I_s \tag{2}$$

$$v(t) = L\frac{dI_s}{dt} + 2R_d I_s + (2U_d + U_c)\,\text{sign}\,(I_s) \tag{3}$$

$$C\frac{dU_c}{dt} + \frac{U_c}{R} = |I_s| \tag{4}$$

The first equation represents the balance of mechanical and electrical forces for the PEH system after reducing the governing partial differential equations into a lumped-parameter form (Roundy, Wright, and Rabaey 2003), where $q, \mu, \omega_0, \vartheta, \Gamma$ are the beam's displacement amplitude, damping, resonant frequency, piezoelectric coupling and modal coupling of the *i-th* mode, respectively. Eq. (2) represents an electrical equation, which results from applying Kirchhoff's current law to node 1 (see Figure 2) in the AC side of the circuit. Eq. (3) represents Kirchhoff's voltage law applied to the whole circuit, being U_d the voltage drop across the diodes of internal resistance R_d and U_c the voltage across capacitor C in the DC side of the circuit. Eq. (4) results from applying Kirchhoff's current law to node 2 in the DC side of the circuit. The parameter β in Eq. (2) represents a correction factor for the non-perpendicularity of the $\boldsymbol{D}$ field in the "1" axis, D_1 which is used to model a piezofiber composite (Bilgen, Erturk, and Inman 2010; Machado et al. 2020).

Parameter estimation of *L*, diode model, experimental validations and comparisons

After presenting the model (Eqs. (1)–(4)), the next step is to determine the parameter values, which are essential to

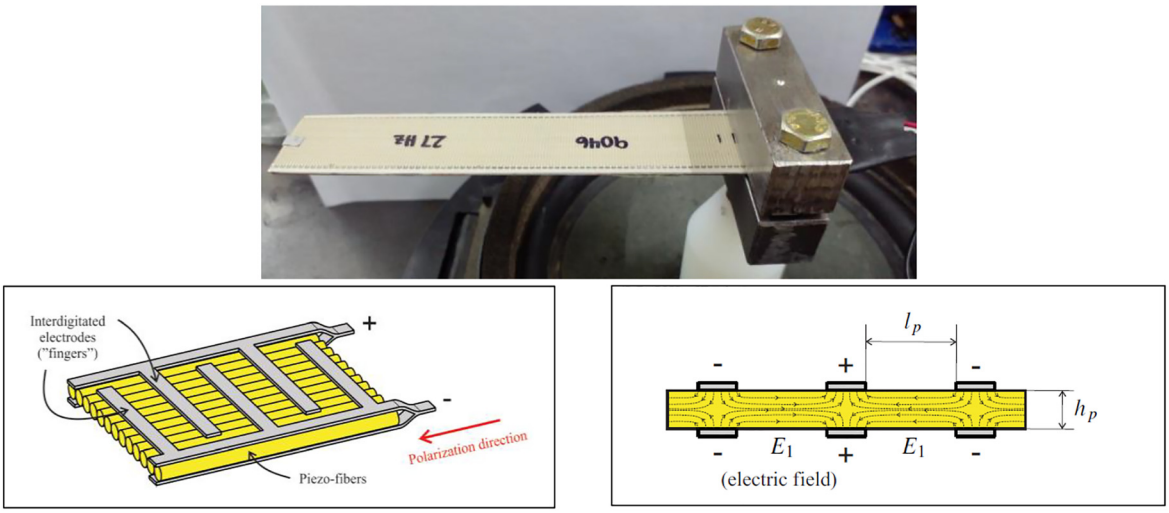

Figure 1: Schematic view of the selected beam of piezofibers composite. Top: real piezofiber composite PFCB-W24 from Advanced Cerametrics Inc. Left: geometric detail of the "fingers" of the electrodes. Right: cross-sectional view of the fibers and electrodes showing the generated electric field.

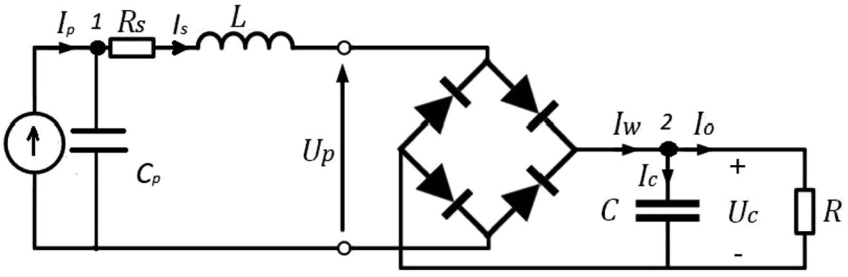

Figure 2: A piezoelectric microgenerator with a full-bridge waveform rectifier (FWR) loaded by a capacitor and a resistor.

calculate the dynamics of the system. Since L counts only for modelling purposes and cannot be found as a real element, its physical value is going to be determined to fit with theoretical, numerical, and experimental predictions.

The selection of the piezoelectric beam of Figure 1 (PFCB-W24), obeys to the following reasons: it offers a high piezoelectric coupling (large voltage for a relative low acceleration) and low resonance frequency, which is very convenient for the study that will be carried out.

The most relevant physical properties of the piezoelectric beam specified in the manufacturer´s data sheet are summarized in Table 1.

Table 1: Material properties for the advanced Cerametrics piezoelectric beam (data sheet).

Advanced Cerametrics	
E_1	30.30 GPa
Density	5440 kg/m^3
Piezoelectric constant d_{31}	−210 pm/V
Resonance frequency	27 Hz
Capacitance (measured)	14.79 nF

Numerical studies

In this subsection, the value of L is going to be determined numerically, using the experimentally identified parameters of the piezoelectric beam (see Linear model of the piezoelectric beam connected to a load resistor: AC response) and solving Eqs. (1)–(4) using a numerical routine. The value of L will be determined by matching the numerical solution with an analytical solution for the DC output voltage of the harvester considering ideal diodes (Steady state: DC response).

Linear model of the piezoelectric beam connected to a load resistor: AC response

As a first step to determine the parameters of the piezoelectric beam, it is connected directly to a load resistor

without the FWR. The following set of linear ordinary differential equations models the system:

$$\ddot{q}(t) + \mu\dot{q}(t) + \omega_0^2 q(t) - \vartheta v(t) = \Gamma a(t) \tag{5}$$

$$C_p \frac{dv(t)}{dt} + \vartheta\beta\dot{q}(t) = -I_s(t). \tag{6}$$

With $I_s(t)$ given by Ohm's law, i.e.,

$$I_s(t) = \frac{v(t)}{R}. \tag{7}$$

Eqs. (5) and (6) can be analytically solved by proposing

$$a(t) = \overline{a}e^{i\Omega t};$$

$$q(t) = \overline{q}e^{i\Omega t};$$

$$v(t) = \overline{v}e^{i\Omega t}.$$

Where $\overline{a}$, $\overline{q}$ and $\overline{v}$ are complex quantities. Finally, for the modulus of the voltage $V = \|\overline{v}\|$, the following expression is obtained:

$$V = \frac{AR\beta\Omega\Gamma\vartheta}{\sqrt{\left(\omega_0^2 - \Omega^2 - 2C_p R\xi\omega_0\Omega^2\right)^2 + \left(2\Omega\xi\omega_0 + R\Omega\left(\vartheta^2 + C_p\omega_0^2 - C_p\Omega_0^2\right)\right)^2}}. \tag{8}$$

Being $A = \|\overline{a}\|$ the amplitude of the base acceleration.

The experimental setup shown in Figure 3 was used to characterize the parameters of the system modeled by Eq. (8).

Figure 3 shows a set of photographs of the setup, which involves a waveform generator (Rigol DG4062) that provides the sinusoidal input, a power amplifier to excite the shaker, an electrodynamic shaker (homemade) for the mechanical acceleration input, a PCB accelerometer (sensitivity of 98.7 mV g^{-1}) attached to the base of the piezoelectric beam to sense the acceleration, and a data acquisition board (NI 9230), that measures the voltage and acceleration signals of the piezoelectric beam using 4096 samples/s.

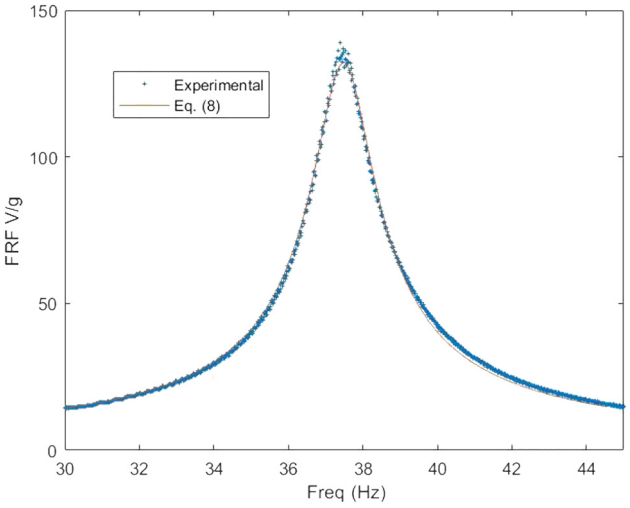

Figure 4: Experimental data and calculated voltage of Eq. (8) for values of Table 2.

Figure 4 shows the experimental data of the voltage/base acceleration, superimposed with the corresponding values calculated with Eq. (7). The experiments were carried out performing a sine-sweep between 30 and 60 Hz, using a 0.05 g base acceleration excitation in order to be within the predictions of the linear theory.

By using the Least Squared Method implemented by Matlab under the curve fitting tool package, the parameters shown in Table 2 were obtained.

These experimentally obtained values will be used in the rest of the sections to validate our proposed model Eqs. (1)–(4).

Steady state: DC response

In the second step, after obtaining the parameters of the piezoelectric beam, the value of L is going to be determined. This task is done by calculating analytically the response of the piezoelectric beam for DC voltage output,

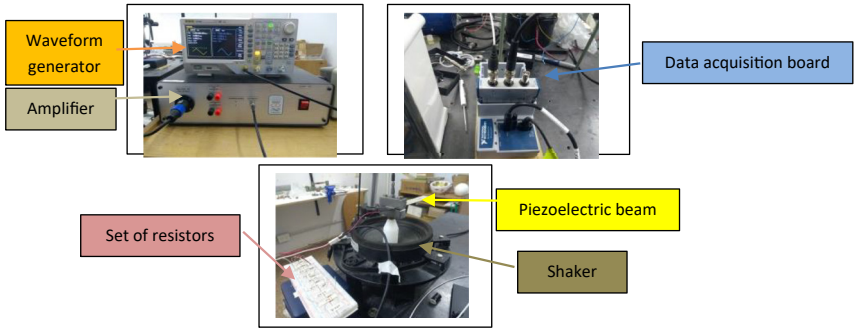

Figure 3: Experimental setup used to determine the parameters of the piezoelectric beam (PFCB-W24).

Table 2: Parameter values obtained by fitting experimental results of Figure 4 and Eq. (7).

Parameter	Value
Γ [adim]	1.23
β [adim]	0.5
$\vartheta\left[\frac{m}{Vs^2}\right]$	0.01
ξ [adim]	0.0062
ω_0 [rad/s];	231.4
f_0 [Hz]	36.82

derived under steady-state base excitation of the form $u(t) = u_0 \sin(\Omega t)$. Following a procedure described in (Shu and Lien 2006), which considers an ideal behavior of the diodes ($U_d = 0$; $R_d = 0$), the value of U_c is obtained, which includes parameter β (not considered in (Shu and Lien 2006)), yielding:

$$U_C = \frac{\vartheta \Omega \beta R}{C_p \Omega R + \frac{\pi}{2}} u_0 \tag{9}$$

where u_0 is given by:

$$u_0 = \frac{\Gamma A}{\sqrt{\left(2\xi\omega_0\Omega + \frac{2\Omega\beta\vartheta^2 R}{\left(C_p\Omega R + \frac{\pi}{2}\right)^2}\right)^2 + \left(\omega_0^2 - \Omega^2 + \frac{\Omega\beta\vartheta^2 R}{\left(C_p\Omega R + \frac{\pi}{2}\right)^2}\right)^2}}.$$

In order to calculate the value of L that best fits the analytically obtained U_C of Eq. (9), Eqs. (1)–(4) were numerically solved using the measured parameter values of the piezoelectric beam given in Table 2, $U_d = 0$; $R_d = 0$ for different values of L ranging from $L = 0.1$; 1; 10; 50; 100 [H] for 40 discrete values of frequency $f = \Omega/(2\pi)$. The numerical routines were implemented in Matlab using the ordinary differential equation solver ODE 45 with $C = 10$ nF and $R = 37{,}500\ \Omega$.

The results of the simulations, together with the analytical predictions of Eq. (9) for different values of L are presented in Figure 5. Generally speaking, it is possible to observe a good matching of the numerical solution for all L's with the analytical model below and above the resonance frequency. In the neighbourhood of resonance, the case $L = 100$ [H] overestimates the analytical solution below and above resonance which is not the case for the other values of L. In those cases, the numerical solutions underestimate the analytical predictions for frequencies below resonance and are larger for frequencies above the resonance frequency of the harvester.

Since it is rather difficult to appreciate how well the approximations are, Figure 6 shows the relative percent error (%) between numerical simulations and Eq. (9), as a function of frequency. Near resonance, all values of L predict similar results (bounded by 25%). For frequencies above resonance, it is possible to see that for $L \geq 50$ [H], the error is increasingly large as we move away from resonance and fluctuates (or remains constant) over an average value for the other cases. Taking into account frequencies below resonance, all values of L present small errors bounded by 5% (except $L = 100$ [H]). By averaging these errors for all frequencies, it is possible to observe that the case $L = 10$ [H] is the value that has the smallest average percent error (approx. 6.38%) in the range 5–75 Hz (see inset of Figure 6).

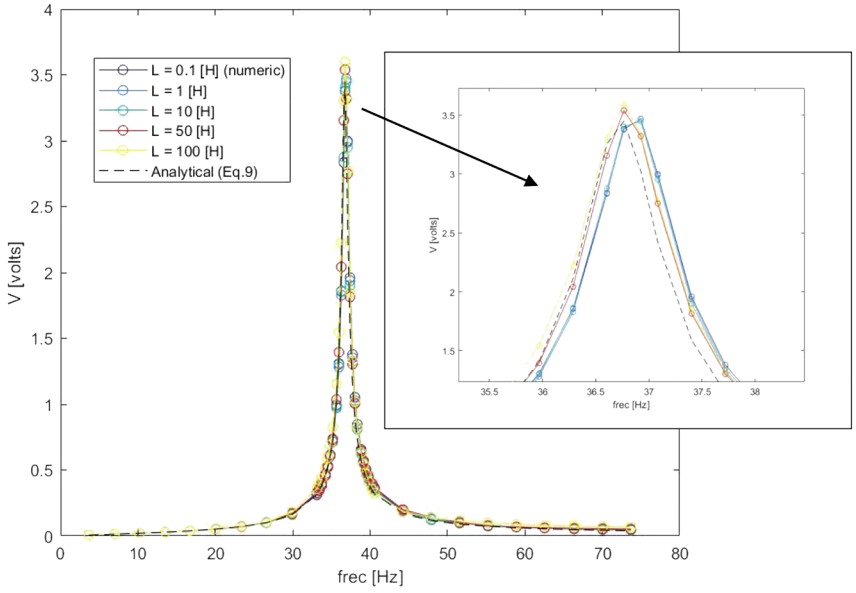

Figure 5: Comparison between Eq. (9) and simulation results of the proposed model for $L = 0.1$; 1; 10; 50; 100 [H] as a function of frequency (Hz) with a zoom near the resonance frequency.

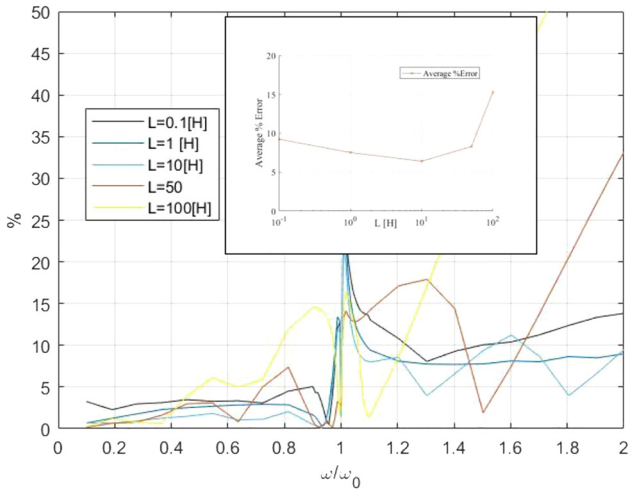

Figure 6: Relative percent error (%) as a function of frequency for different values of L. Inset, average percent error as a function of L.

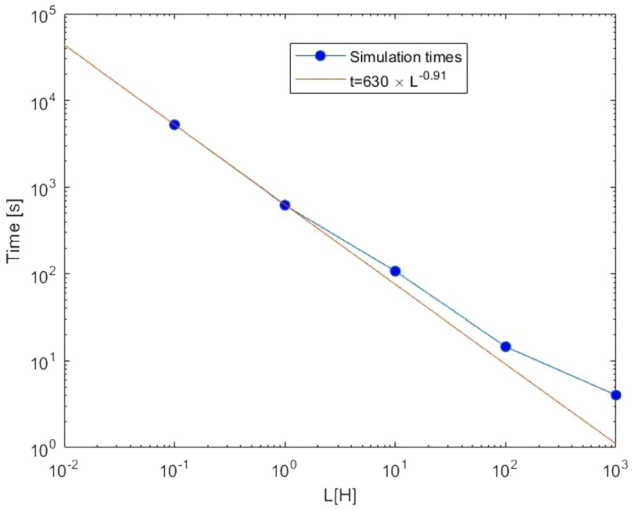

Figure 7: Simulation times as a function of L. The solid line represents a nonlinear fit for an analytical estimation.

Values of L and simulation times

It is worth to ask whether it is possible to consider lower or larger values of L in the simulations of the previous section. In this sense, this subsection pretends to give physical insight into this question by inspecting the simulation times required to reach a steady-state solution under a sinusoidal excitation. From a computational point of view, a large simulation time means that the algorithm (ODE 45 with adaptive time steps) uses tiny time steps from the initial time to the final time in order to satisfy a fixed relative and absolute tolerances (which is a standard scaling of an accurate integration). So, if there exist significant variations in the piezo voltage, $v(t)$, a small value of L means that the output voltage, U_c, must suffer large variations after the nonlinear AC-DC conversion process carried out by the diodes Consequently, it requires tiny time steps to converge, resulting in large simulation times. On the contrary, a large value L means shorter simulation times to solve the nonlinear AC-DC conversion, since the inductor term absorbs the significant variations in $v(t)$ (smoothing the current that flows through the diodes). However, an extremely large value of L gives inaccurate results, as demonstrated by Figure 6.

Figure 7 represents the simulation time required to solve Eqs. (1)–(4) for $a(t) = A\,\sin(\omega_0 t)$ (resonant base excitation) for different values of L and a curve fitting for their analytical estimation. The parameters of the system are the same as used in Steady state: DC response. It can be observed that the value of the simulation time increases as an inverse power of L supporting the above discussion. At the same time, large values of L produce inaccurate results which means that there exists a trade-off between accuracy and fast convergence of the results.

The assumption of the value of the inductor (L) obtained in Steady state: DC response remains valid as soon as its impedance satisfies $Z_L < Z_R$ (Z_R the rectifier input impedance). Since $Z_L = \Omega L$ this is equivalent to saying that

$$\Omega < \frac{Z_R}{10\ [\mathrm{H}]} \tag{10}$$

Then, for periodic/non-periodic excitations, we must ensure that the maximum spectral component (frequency) of the excitation satisfies Eq. (12) in order to have a minimum impact in the output DC voltage of the harvester.

Diode model

Steady state: DC response uses ideal diodes ($U_d = 0$; $R_d = 0$) to determine the values of L since the analytical formulation (Eq. (8)) disregards the real behavior of the diodes. However, in order to model the nonlinear characteristics of a real diode included in the proposed model (Eqs. (1)–(4)), we adopt a piecewise linear (PWL) model (Sedra and Smith 2004) for the diodes. This model approximates the diode's nonlinear voltage-current behavior as a constant voltage source, U_d, in series with a resistor, R_d. Figure 8 shows a real diode I–V curve using the Shockley diode model, that relates the voltage across the diode, v_D, to the current that flows through it, i_D, defined by the following relation:

$$i_D = I_S\left[e^{v_D/nV_T} - 1\right].$$

Where I_S is the saturation current, n is the ideality factor and V_T is the thermal voltage. The numerical values of I_S, n, V_T for the numerical examples presented in this article are:

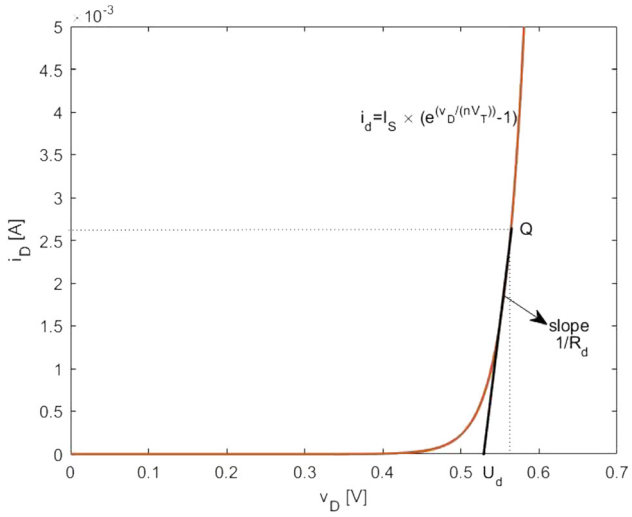

Figure 8: *I–V* curve of the Shockley model of a real diode. U_d and R_d as obtained by the piecewise linear approximation (PWL).

$I_S = 10^{-12}$[A]; $n = 1$; $V_T = 26 \times 10^{-3}$[V]. At the same time, a two-segment piecewise linear model is shown for comparison. The value of R_d is calculated by the reciprocal of the slope of i_D versus v_D at the operating point, or Q-point, and U_d is the intersection of this tangent line with the v_D axis. Finally, it is straightforward to obtain the analytical expressions for R_d and U_d in terms of i_D as follows:

$$R_d = \frac{nV_T}{I_S} \frac{e}{\left(\frac{i_D}{I_S} + 1\right)} \tag{11}$$

$$U_d = v_D - i_D R_d = nV_T \ln\left(\frac{i_D}{I_S} + 1\right) - i_D R_d \tag{12}$$

It is important to note that since the current that flows through the diodes (I_s in Eqs. (1)–(4))can take alternatively positive and negative values in this model, the absolute value of this current will be considered in Eqs. (11) and (12) for the simulations in Eqs. (1)–(4) in order to prevent negative values of R_d and U_d.

Experimental validations: transient response under sinusoidal excitation

In order to make a first test to investigate the validity of the inductance value obtained in Steady state: DC response using the diode model of Diode model, an experimental test is carried out to validate the numerical simulations.

The experimental setup is the same as the one displayed in Figure 3, adding this time a FWR, a capacitor C, and a resistor R, as shown in Figure 2.

A sinusoidal acceleration of frequency 40 Hz and amplitude 0.1 g is suddenly applied from zero, to excite the base of the piezoelectric beam, as shown in Figure 9(a). Figure 9(b) shows the experimental DC output voltage developed across resistor R. There, it is possible to observe an increasing voltage from zero up to the steady-state DC voltage of approximately 1 V. During the initial transient, capacitor C charges with current I_C until it reaches the steady-state, approximately after 0.6 s.

In order to obtain a numerical estimation for the DC values, Eqs. (1)–(4) were numerically solved using the same routine described in Steady state: DC response. The value of U_d and R_d are given by Eqs. (10) and (11) in terms of the diode's current. The parameter values for the simulations are given by Table 2 and $C = 10$ μF and $R = 37.5$ kΩ. In this case, the acceleration introduced in the simulations was the measured acceleration of Figure 9(a). The results are shown in Figure 10, where different values of L were tested: $L = 100$; 50; 10; 1; 0.1 [H].

Model predictions match very well with the experimental data, with an average value of the (absolute) difference between the experimental and numerical solution no larger than 0.11 V (or 10% of the peak voltage) in the worst-case $L = 100$ [H]. It is important to note that the case of $L = 50$ [H]gives the least (average) difference, in agreement with Figure 6 for frequencies just above resonance, as in this case of single frequency excitation (40 Hz).

Comparison with other formulations: steady state

In a recent paper, Leadenham and Erturk (2020) represented a resonant piezoelectric beam with mechanical and dissipative nonlinearities as well as the nonlinear process of AC–DC conversion with nonideal diodes, using a harmonically externally excited PEH. They predict the DC voltage across the load in terms of the AC mechanical input (base vibration) and arrived at the following equations (Eqs. (30)–(32)) of Ref (Leadenham and Erturk 2020), where material and geometric nonlinearities have been arbitrarily disregarded in this case, to make a fair comparison with our proposed model:

$$\ddot{q}(t) + \mu\dot{q}(t) + \omega_0^2 q(t) - \vartheta v(t) = \Gamma a(t) \tag{13}$$

$$C_p \frac{dv(t)}{dt} + \vartheta\beta\,\dot{q}(t) = -2I_S \sinh\left(\frac{v(t)}{2nV_T}\right) e^{-(U_C/2nV_T)} \tag{14}$$

$$C\frac{dU_c}{dt} + \frac{U_c}{R} = -2I_S\left[1 - \cosh\left(\frac{v(t)}{2nV_T}\right) e^{-(U_C/2nV_T)}\right] \tag{15}$$

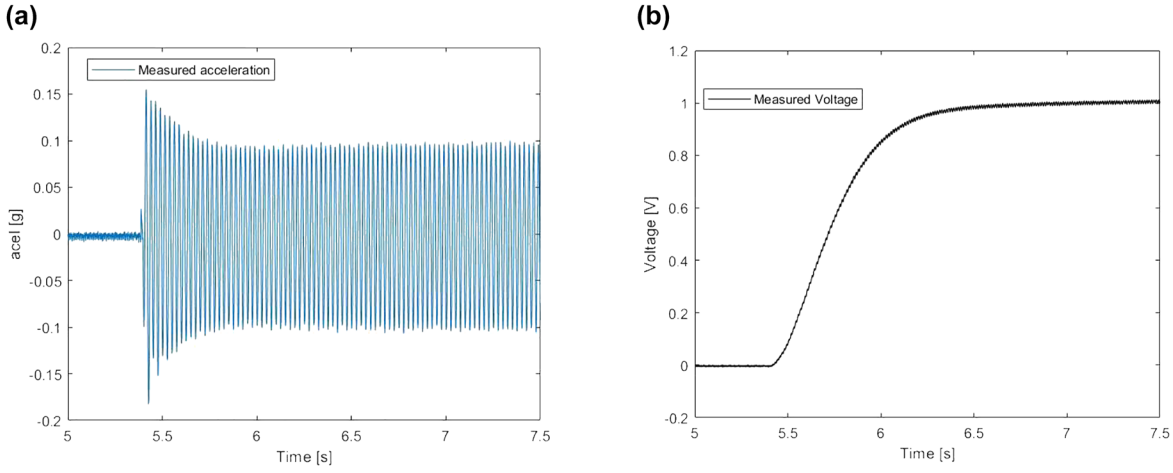

Figure 9: Transient response under sinusoidal excitation. (a) Base acceleration input applied at 5.4 s with freq. 40 Hz (near resonance) and amplitude 0.1 g; (b) experimental output voltage U_c after the FWR (schematics in Figure 2).

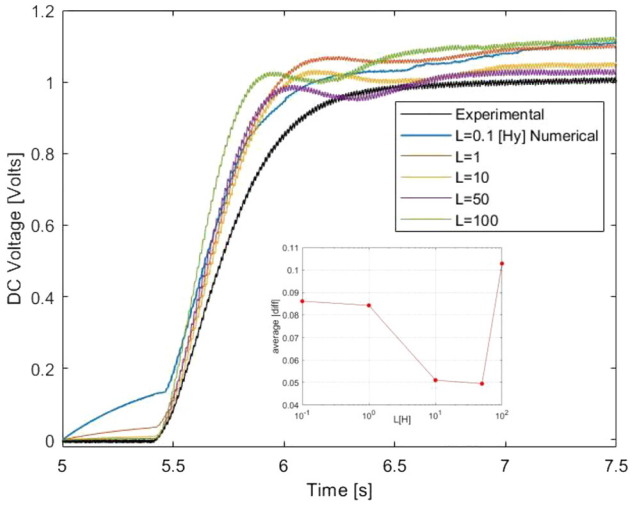

Figure 10: Comparison between experimental and numerical results from different values of inductances. Inset, average of the absolute difference between the experimental and numerical solutions.

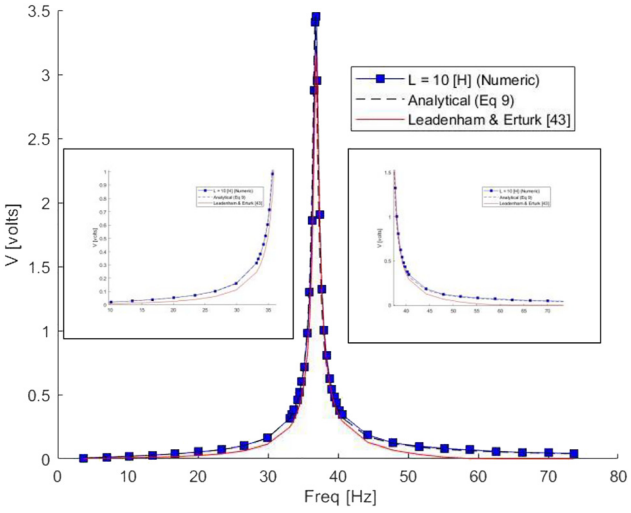

Figure 11: Comparison between Leadenham and Erturk (2020), the proposed formulation with L = 10 [H] and Eq. (9).

Shockley diode modelling was also used.

Figure 11 presents a comparison between our formulation, using the same parameters of Comparison with the proposed model with L = 10 [H], the approach of Leandenham & Erturk and the analytical approach of Eq. (9). It is possible to observe good agreement for frequencies near resonance for the three approaches. However, for frequencies above or below resonance, ref (Leadenham and Erturk 2020) presents some differences compared with the analytical formulation (see inset in Figure 11). These differences come from considering ideal diodes in the analytical formulation (Eq. (9)) which cannot be introduced as a limiting case in Eqs. (13)–(15). On the contrary, it is straightforward to consider ideal diodes in the present formulation making U_d = 0 and R_d = 0 in Eq. (3).

Figure 12 represents the percent error (difference between the simulations and the analytical formulation of Eq. (9)) as a function of frequency. It is possible to observe some discrepancies in the formulation of ref (Leadenham and Erturk 2020) for frequencies far from resonance. The average value of this error, considering the whole range of frequencies, is 6.38% for the proposed formulation and 35.45% for ref (Leadenham and Erturk 2020). It is important to recall that the Shockley model gives tiny voltage drops corrections for frequencies far above or below resonance since the current generated by the piezoelectric system for these frequencies is extremely small and, consequently, the voltage drops in the diodes are small too, approximating an ideal behavior.

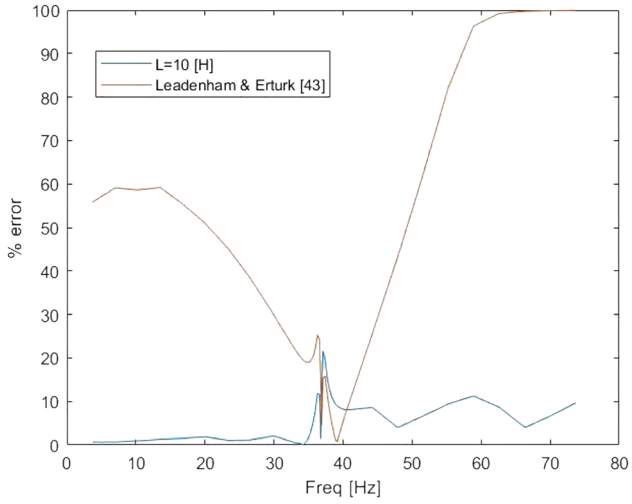

Figure 12: Percent error between Leadenham and Erturk (2020), the proposed formulation with $L = 10$ [H] and the analytical formula Eq. (9).

Real case acceleration excitation

For a final test for the proposed formulation, a PEH-FWR and an accelerometer were mounted on a bike as an experimental setup for a real case (arbitrary) acceleration excitation, as shown in Figure 13a and b. Figure 13a is a photo of the device that measures the acceleration and the DC output voltage of the PEH. It consists of an ATMEGA-based data acquisition system (Analog to digital converter) that samples the signal of an MPU-6050 accelerometer at a rate of 500 samples/s and at the same time samples the DC output voltage from the analog inputs A0, A1 of the ATMEGA microprocessor with the same data rate.

The measured acceleration and voltage are shown in Figure 14a and b, respectively, for the first 60 s.

In order to have an independent numerical prediction of the rectified output voltage, a LTspice simulation was made for the case of Figure 14(a) and (b).

The circuit is nonlinear and time-variant due to the diode bridge rectifier, as modeled by Eqs. (1)–(4). LTspice can solve for the transient and steady-state responses using various models of the semiconductors; in this case, the diodes were represented by their Shockley model.

The sampled data were stored in a .wav file used as the excitation input. The .wav file data points are limited to ±1V; thus, the original data points were manipulated to fit in that range and then scaled back up in E_1. The PEH was modeled by its electric analogy as described in (Pinna, Dahiya, and Valle 2009). The equivalent circuit model is shown in Figure 15, where the mechanical part is represented by E_1, L_2, R_b and C_2; while the electromechanical conversion is modeled by $B_1$and B_2. Voltage source E_1 takes into account the mechanical excitation, L_2 represents the system´s mass, R_{pri} the damping, C_2 the spring constant and the controlled sources, $B_1$and B_2, the electromechanical energy conversion; finally, C_b models the output capacitor of the PEH. The energy harvesting circuit is completed with the diode bridge rectifier (D_1–D_4), the filter capacitor (C_3) and the load resistor (R_1). The diodes were modeled using the same saturation current and ideality factor that was used for their PWL model; a large resistor (170 kΩ) was connected in parallel with each diode to account for the inverse current allowed by the implemented PWL approximation Eqs. (10) and (11).

Comparison with the proposed model

The voltage comparison between the numerical LTspice model, the proposed model with $L = 10$ [H], the model of Leadenham and Erturk (2020), and experimental values are presented in Figure 16a. with an input acceleration given by Figure 16b (bike measurements). At first sight, it is possible to observe a qualitative coincidence between the three numerical formulations. Comparing those with the

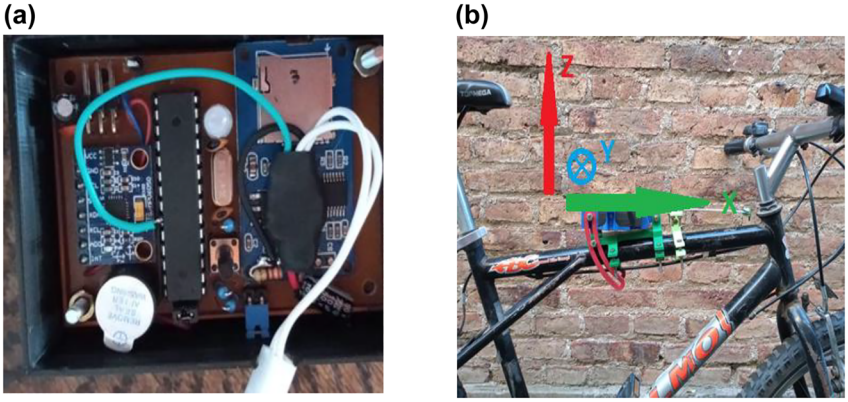

Figure 13: Real case acceleration excitation. Measurement device. (a) Measurement device for the acceleration and voltage, (b) experimental setup of the measurements on a bike.

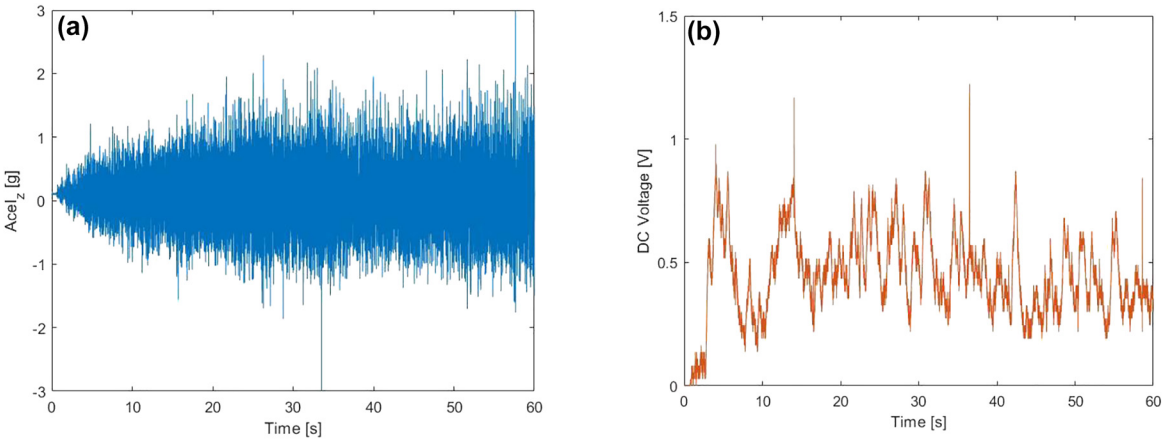

Figure 14: Real case acceleration excitation. Measurements. (a) Measured acceleration (in g units) up to 60 s and (b) DC voltage of a real case acceleration (bike).

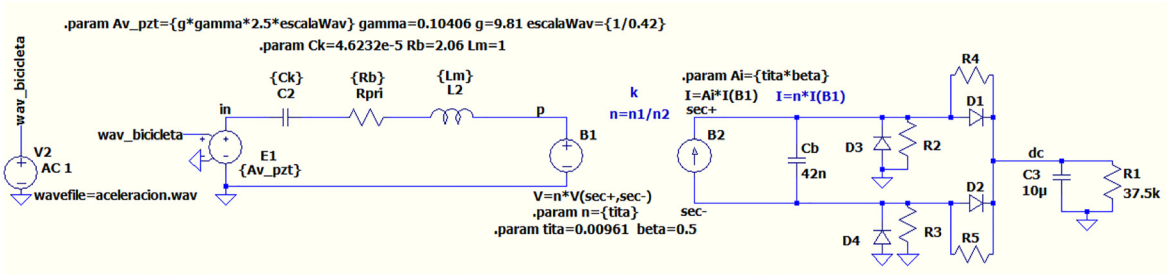

Figure 15: LTspice model of the piezoelectric system modeled by Eqs. (1)–(4).

experimental data, there exist some discrepancies, which can be in part attributed to several issues: a nonlinear increasing error with amplitude in the analog-to-digital conversion based on the ATMEGA microprocessor, errors in the measured acceleration due to the MPU-based accelerometer, errors due to a low sampling rate (500 samples/s).

Regarding our proposed numerical scheme $L = 10$ [H] (in Figure 16), using U_d and R_d as stated in Eqs. (10) and (11), it is possible to observe that it reaches almost an

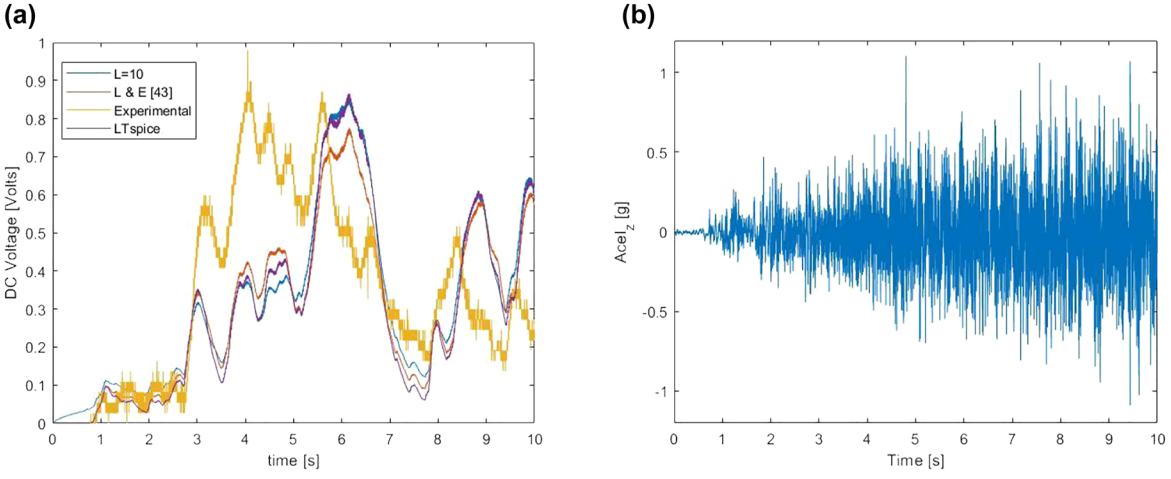

Figure 16: Real case acceleration excitation. Comparisons. (a) Comparison between experimental, numerical and LTspice simulation of the voltage values of the PEH-FWR system under the real case acceleration measurements of (b).

identical value for the peak voltage (experimental = 0.87 V, numerical = 0.85 V) and it can copy the increments and decrements of the experimental voltage for the complete interval. It is important to note that not the present nor the other numerical formulations match well with the first ramp of the experimental voltage (starting approx. at 3 s), indicating that there exist some experimental conditions not considered in the model.

As another validation of the proposed formulation, the time integral of the instantaneous output power is calculated across the load resistance of 37.5 kΩ for a considered time interval $(0, t_f)$:

$$E = \int_0^{t_f} \frac{U_c^2}{R} \mathrm{d}t. \tag{16}$$

The time integral of the power may be thought of as the total energy transferred to the resistance up to a certain time and provides a means of quantifying the output energy of the harvester. In this sense, this cumulative energy can be used as a performance index for the numerical model. Upon making a comparison of the first 10 s ($t_f = 10\,s$), the computed energy for the experimental results gives 47.1 μJ, and the calculated energy from the numerical model is 40.43 μJ. This result represents a difference of less than 14.2%. Compared with the case of ref (Leadenham and Erturk 2020), with an error of 24.4%, our model represents a good estimation of the output energy transferred to the resistance of a PEH with a FWR for an arbitrary excitation input.

Ideal, low-biased and forward-biased diodes

One of the main advantages of the present formulation (Eqs. (1)–(4)) compared to the previous one (Leadenham and Erturk 2020) is that it is possible to consider a different average behavior of the diodes depending on the impact of their voltage drop on the DC voltage. For instance, if the piezoelectric transducer's output voltage is high compared to the voltage drop across the diode, an ideal diode model (no voltage drop) can be used. If the voltage drop across the diode is comparable to the output voltage of the piezoelectric transducer, then its voltage drop can be taken into account depending if it is low-biased or forward biased, simply by adapting the values of U_d and R_d according with the operating point. Table 3 shows four possible set of values, and Figure 17 present a comparison of the four cases with the actual case acceleration measurements of Figure 16b.

Figure 17 presents the results for the 4 cases. As expected, since the piezoelectric transducer's output voltage is comparable to the voltage drop across the diode, an ideal diode model gives inaccurate results compared with the experimental case. On the contrary, a low-biased diode gives a better approximation to the case of variable voltage-current characteristics of a real diode, such as the one considered in the present article.

Table 3: Three cases of U_d and R_d considered to replicate ideal, low-biased and forward biased diodes.

Case	U_d [Volts]	R_d [Ohms]	Simulation time (normalized)
Ideal	0	0	1.0
Low-biased	0.543	6398	1.9
Forward-biased	0.7	0	2.8
Variable	Eq. (10)	Eq. (11)	2.0

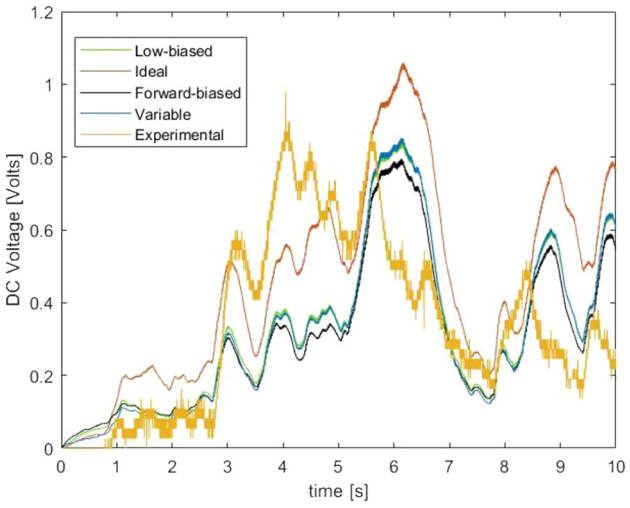

Figure 17: Comparison between experimental and three cases for the numerical modelling: ideal diodes, low-biased and forward biased diodes.

Conclusions

This article presents a set of nonlinear differential equations to obtain the DC voltage of a piezoelectric energy harvesting system with a full-bridge waveform rectifier loaded with a capacitor in parallel with a resistor, for an arbiratry base excitation. The amplitude of the excitation is kept low enough for the system to operate in the linear region. This is done to study the effect of the nonlinear AC-DC process provided by the FWR in the voltage generation of a PEH. The model introduces an inductor to smooth the current under rapid variations of the piezoelectric current, and a piecewise linear model for real diodes. The

main advantage of this modelling lies in being able to consider different operating points for the diodes easily.

The value of the inductor is obtained by minimizing the difference between the voltage values obtained by the simulations and the exact analytical result for a steady-state excitation considering ideal diodes. The voltage drop in the diodes and their resistances, which are also parameters of model, are obtained from the proposed piecewise linear model using the Shockey model.

Several comparisons have been made to validate proposed model: with an experimental test of transient base acceleration, with a previous numerical formulation and with a random excitation test provided by the acceleration of a bicycle. This last result is also compared using commercial software LTspice.

All these tests agree with the proposed model for the selected value of the inductor and the proposed voltage drops and resistances of the diodes. Moreover, the model can be adapted and provide good estimations when considering different operating points for the diodes (low or forward biased) as have been demonstrated compared with the bike case. In summary, the proposed formulation can be used as a numerical tool to predict the output voltage and energy for a large range of excitation frequencies, including resonant and nonresonant conditions and ideal and non-ideal diodes for general piezoelectric systems under arbitrary base input excitations.

Author contributions: All the authors have accepted responsibility for the entire content of this submitted manuscript and approved submission.

Research funding: The authors would like to thank the financial support from CONICET, Universidad Nacional del Sur under grant PGI 24/F077, Universidad Tecnológica Nacional and FONCYT under grant PICT-2017-0688.

Conflict of interest statement: The authors declare no conflicts of interest regarding this article.

References

Anton, S. R., and H. A. Sodano. 2007. "A Review of Power Harvesting Using Piezoelectric Materials (2003–2006)." *Smart Materials and Structures* 16: R1–24.

Ayala-Garcia, I., D. Zhu, M. Tudor, and S. Beeby. 2010. "A Tunable Kinetic Energy Harvester With Dynamic Over Range Protection." *Smart Materials and Structures* 19 (11): 1–10.

Beeby, S. P., M. J. Tudor, and N. M. White. 2006. "Energy Harvesting Vibration Sources for Microsystems Applications." *Measurement Science and Technology* 17: R175–95.

Bertotti, G., and I. D. Mayergoyz. 2006. *The Science of Hysteresis: Hysteresis in Materials*, Vol. 3. Amsterdam: Elsevier.

Bilgen, O., A. Erturk, and D. J. Inman. 2010. "Analytical and Experimental Characterization of Macro-Fiber Composite Actuated Thin Clamped-free Unimorph Benders." *Journal of Vibration and Acoustics* 132: 051005.

Chen, C.-D., Y.-H. Wu, and P.-W. Su. 2020. "Dynamic Modeling and Experimental Validation of an Impact-Driven Piezoelectric Energy Harvester in Magnetic Field." *Sensors* 20 (21): 6170.

Clementino, M. A., R. Reginatto, and S. da Silva. 2014. "Modeling of Piezoelectric Energy Harvesting Considering the Dependence of the Rectifier Circuit." *Journal of the Brazilian Society of Mechanical Sciences and Engineering* 36: 283–92.

Daqaq, M., C. Stabler, Y. Qaroush, and T. Seuaciuc-Osorio. 2009. "Investigation of Power Harvesting via Parametric Excitations." *Journal of Intelligent Material Systems and Structures* 20 (5): 545–57.

Erturk, A., and D. J. Inman. 2008. "A Distributed Parameter Electromechanical Model for Cantilevered Piezoelectric Energy Harvesters." *Journal of Vibration and Acoustics* 130: 041002.

Erturk, A., and D. J. Inman. 2011. *Piezoelectric Energy Harvesting*. Chichester, UK: John Wiley & Sons, Ltd. ISBN: 978-0-470-68254-8.

Fan, F. R., W. Tang, and Z. L. Wang. 2016. "Flexible Nanogenerators for Energy Harvesting and Self-Powered Electronics." *Advanced Materials* 28: 4283–305.

Febbo, M., and S. P. Machado. 2022. "Rotational Multi-Beam Energy Harvester With Up-Conversion Mechanism in an Extremely Low Frequency Scenario." *Mechanical Systems and Signal Processing* 168: 108737.

Fu, H., X. Mei, D. Yurchenko, S. Zhou, S. Theodossiades, K. Nakano, and E. M. Yeatman. 2021. "Rotational Energy Harvesting for Self-Powered Sensing." *Joule* 5: 1–45.

Gatti, C. D., J. M. Ramirez, M. Febbo, and S. P. Machado. 2018. "Multimodal Piezoelectric Device for Energy Harvesting from Engine Vibration." *Journal of Mechanics of Materials and Structures* 13: 17–34.

Goldschmidtboeing, F., C. Eichhorn, M. Wischke, M. Kroener, and P. Woias. 2011. "The Influence of Ferroelastic Hysteresis on Mechanically Excited PZT Cantilever Beams." In *Proc. of the 11th Int. Workshop on Micro and Nanotechnology for Power Generation and Energy Conversion Applications*, 114–7.

Gu, L. 2011. "Low-frequency Piezoelectric Energy Harvesting Prototype Suitable for the MEMS Implementation." *Microelectronics Journal* 42: 277–82.

Gu, L., and K. Livermore. 2011. "Impact-Driven, Frequency Up-Converting Coupled Vibration Energy Harvesting Device for Low Frequency Operation." *Smart Materials and Structures* 20: 10, 045004.

Halim, M. A., H. O. Cho, and J. Y. Park. 2015. "A Handy Motion Driven, Frequency Up-Converting Piezoelectric Energy Harvester Using Flexible Base for Wearable Sensors Applications." In *IEEE Proceedings*.

Harb, A. 2011. "Energy Harvesting: State-Of-The-Art." *Renewable Energy* 36: 2641–54.

Jia, Y., and A. Seshia. 2014. "An Auto-Parametrically Excited Vibration Energy Harvester." *Sensors and Actuators, A: Physical* 220: 69–75.

Joshi, S. P. 1992. "Non-linear Constitutive Relations for Piezoceramic Materials." *Smart Materials and Structures* 1: 80.

Kurmann, L., Y. Jia, Y. Manoli, and P. Woias. 2016. "Magnetically Levitated Autoparametric Broadband Vibration Energy Harvesting." *Journal of Physics: Conference Series* 773: 012006.

Kathpalia, B., D. Tan, I. Stern, and A. Erturk. 2018. "An Experimentally Validated Model for Geometrically Nonlinear Plucking-Based Frequency Up-Conversion in Energy Harvesting." *Smart Materials and Structures* 27 (1): 015024.

Leadenham, S., and A. Erturk. 2020. "Mechanically and Electrically Nonlinear Non-Ideal Piezoelectric Energy Harvesting Framework With Experimental Validations." *Nonlinear Dynamics* 99 (1): 625–41.

Machado, S. P., M. Febbo, C. D. Gatti, and S. M. Osinaga. 2020. "A Piezoelectric Beam Model With Geometric, Material and Damping Nonlinearities for Energy Harvesting." *Smart Materials and Structures* 29 (9): 095009.

McInnes, C., D. Gorman, and M. Cartmell. 2008. "Enhanced Vibrational Energy Harvesting Using Nonlinear Stochastic Resonance." *Journal of Sound and Vibration* 318 (4–5): 655–62.

Mei, X., S. Zhou, Z. Yang, T. Kaizuka, and K. Nakano. 2021. "Enhancing Energy Harvesting in Low-Frequency Rotational Motion by a Quad-Stable Energy Harvester with Time Varying Potential Wells." *Mechanical Systems and Signal Processing* 148: 107167.

Moehils, J., J. Rogers, B. DeMartini, and K. Turner. 2009. "Exploiting Nonlinearity to Provide Broadband Energy Harvesting." In *Proc. ASME DSCC, Hollywood, California, USA, Oct 12 – 14*, 3.

Mori, K., T. Horibe, S. Ishikawa, Y. Shindo, and F. Narita. 2015. "Characteristics of Vibration Energy Harvesting Using Giant Magnetostrictive Cantilevers With Resonant Tuning." *Smart Materials and Structures* 24: 125032 (7pp).

Peano, F., and T. Tambosso. 2005. "Design and Optimization of a MEMS Electret-Based Capacitive Energy Scavenger." *Journal of Microelectromechanical Systems* 14: 429–35.

Pinna, L., R. S. Dahiya, and M. Valle. 2009. "SPICE Model for Piezoelectric Bender Generators." In *2009 16th IEEE International Conference on Electronics, Circuits and Systems – (ICECS 2009)*, 587–90.

Ramírez, J. M., C. D. Gatti, S. P. Machado, and M. Febbo. 2017. "An Experimentally Validated Finite Element Formulation for Modeling 3D Rotational Energy Harvesters." *Engineering Structures* 153: 323–31.

Ramírez, J. M., C. D. Gatti, S. P. Machado, and M. Febbo. 2019. "A Piezoelectric Energy Harvester for Rotating Environment Using a Linked E-Shape Multi-Beam." *Extreme Mechanics Letters* 27: 8–19.

Roundy, S., and J. Tola. 2013. "An Energy Harvester for Rotating Environments Using Ofset Pendulum Dynamics." In *Transducers and Sensors, Barcelona, Spain, June 16–20*, 689–92.

Roundy, S., P. K. Wright, and J. M. Rabaey. 2003. *Energy Scavenging for Wireless Sensor Networks*. Boston, MA: Kluwer Academic.

Saravia, C. M., J. M. Ramírez, and C. D. Gatti. 2017. "A Hybrid Numerical-Analytical Approach for Modeling Levitation Based Vibration Energy Harvesters." *Sensors and Actuators, A: Physical* 257: 20–9.

Sedra, A. S., and K. C. Smith. 2004. *Microelectronic Circuits*, 5th ed. New York: Oxford.

Shahab, S., S. Zhao, and A. Erturk. 2018. "Soft and Hard Piezoelectric Ceramics and Single Crystals for Random Vibration Energy Harvesting." *Energy Technology* 6 (5): 935–42.

Shu, Y. C., and I. C. Lien. 2006. "Analysis of Power Output for Piezoelectric Energy Harvesting Systems." *Smart Materials and Structures* 15: 1499–512.

Stanton, S. C., A. Erturk, B. P. Mann, and D. J. Inman. 2010. "Nonlinear Piezoelectricity in Electroelastic Energy Harvesters: Modeling and Experimental Identification." *Journal of Applied Physics* 108: 074903.

Stanton, S., C. McGehee, and B. Mann. 2009. "Reversible Hysteresis for Broadband Magnetopiezoelastic Energy Harvesting." *Applied Physics Letters* 95 (17): 3.

Upadrashta, D., and Y. Yang. 2016. "Experimental Investigation of Performance Reliability of Macro Fiber Composite for Piezoelectric Energy Harvesting Applications." *Sensors and Actuators, A: Physical* 244: 223–32.

Wang, Z., T. Li, Y. Du, Z. Yan, and T. Tan. 2021. "Nonlinear Broadband Piezoelectric Vibration Energy Harvesting Enhanced by Inter-well Modulation." *Energy Conversion and Management* 246: 114661.

Wang, M., P. Yina, Z. Li, L. Suna, J. Dinga, L. Luoa, S. Xiea, Y. Penga, and H. Pua. 2020. "Harnessing Energy From Spring Suspension Systems With a Compressive-Mode High-Power-Density Piezoelectric Transducer." *Energy Conversion and Management* 220: 113050.

Wciślik, M., and P. Strząbała. 2016. "The Simulation Analysis of the Bridge Rectifier Continuous Operation in AC Circuit." *Computer Applications in Electrical Engineering* 14: 53–65.

Wu, W. J., A. M. Wickenheiser, T. Reissman, and E. Garcia. 2009. "Modeling and Experimental Verification of Synchronized Discharging Techniques for Boosting Power Harvesting From Piezoelectric Transducers." *Smart Materials and Structures* 18 (5): 055012.